Steam-activated sawdust efficiency in treating wastewater contaminated by heavy metals and phenolic compounds

Noureddine Elboughdiri, Babar Azeem, Djamel Ghernaout, Saad Ghareba and Karim Kriaa

ABSTRACT

This research study encompasses the utilization of new adsorbents fabricated from pine sawdust for the adsorption of heavy metals and phenol from simulated industrial wastewater. Batch trials are conducted to evaluate the activity of these adsorbents for a possible substitution of the costly commercial adsorbents. The maximum adsorption capacities are evaluated and linked to the physicochemical characteristics of the adsorbents. The maximum monolayer adsorption capacity (q_{max}) of the adsorbents corresponds to the specific surface area of the adsorbents. The adsorbents with the larger specific surface area have shown higher q_{max} estimates (phenol adsorption is an exception). The highest amount of the phenol pollutant adsorbed by steam-activated sawdust (SAS) is 10.0 mg/g. The performance of SAS is found to be of the same order as the commercial activated carbon for the removal of Pb and Zn. Equilibrium data for the metal removal are in concordance with the Freundlich adsorption isotherm, whereas the phenol elimination has satisfied the Langmuir adsorption isotherm model. Kinetic data are fitted to Lagergren pseudo-first-order, pseudo-second-order, and the intraparticle diffusion models. Thus, kinetic parameters, rate constants, equilibrium adsorption capacities, and related correlation coefficients for each kinetic model are determined and discussed. The results suggest that the adsorption of Cr follows pseudo-second-order kinetics, indicating chemisorption for the tested adsorbents such that the intraparticle diffusion is not the only step that controls the overall process for Cr adsorption. At the end of this study, the production cost of the SAS adsorbent is estimated ($52 per kg) and compared to the cost of the commercial AC adsorbent in the industrial sector which has a great variation ($80–300 per kg) based on size and location plant. The results of this study can be used for the design of a suitable ecological control procedure to mitigate the harmful effects of industrial wastewater.

Key words | activated carbon (AC), adsorption, heavy metals, kinetics, phenol, steam-activated sawdust (SAS)

HIGHLIGHTS

- The effects of several parameters, including the pH, temperature, initial phenol concentration, and contact time, should be investigated, and the desirable adsorption conditions, the adsorption kinetics model, and the equilibrium model for heavy metals and phenol will be selected.
- The steam-activated sawdust adsorbent could be a promising solution to the removal of heavy metals and phenol from industrial wastewater.

Noureddine Elboughdiri (corresponding author)
Djamel Ghernaout
Saad Ghareba
Chemical Engineering Department,
College of Engineering,
University of Ha'il,
P.O. Box 2440, Ha'il 81441,
Saudi Arabia
E-mail: *ghilaninouri@yahoo.fr*

Noureddine Elboughdiri
Chemical Engineering Process Department,
National School of Engineering Gabes,
University of Gabes,
Gabes 6011,
Tunisia

Babar Azeem
Department of Chemical Engineering,
The University of Faisalabad, Engineering Wing,
West Canal Road, P. O. Box. 38070, Faisal Town,
Faisalabad,
Pakistan

Djamel Ghernaout
Faculty of Engineering, Chemical Engineering Department,
University of Blida,
P.O. Box 270, Blida 09000,
Algeria

Saad Ghareba
Department of Chemical and Petroleum Engineering,
ElMergib University,
Alkhums,
Libya

Karim Kriaa
Chemical Engineering Department, College of Engineering,
Imam Mohammad Ibn Saud Islamic University,
Riyadh 11432,
Saudi Arabia

doi: 10.2166/wrd.2021.114

NOMENCLATURE

Symbol	Description and (Units)
C_e	Equilibrium liquid-phase solute concentration (mg/L)
C_o	Initial liquid-phase solute concentration (mg/L)
C_t	Liquid-phase solute concentration at time, t (mg/L)
k	Number of independent variables (/)
k_{ad}	Pseudo-first-order rate constant (min^{-1})
K_F	Freundlich constant related with adsorption capacity (mg/g)
k_{id}	Intraparticle diffusion rate constant ($mg/g\ min^{1/2}$)
K_L	Langmuir affinity constant (l/mg)
k_2	Pseudo-second-order rate constant ($g\ mg^{-1}\ min^{-1}$)
m	Mass of dry adsorbent (g)
n	Adsorption intensity (/)
P_r	Percentage removal (%)
q_e	Equilibrium adsorption capacity (mg/g)
q_{max}	Maximum monolayer adsorption capacity (mg/g)
q_t	Amount of solute adsorbed at time, t (mg/g)
R^2	Correlation coefficient (/)
S_{BET}	BET surface area (m^2/g)
Smi	Micropore-specific area (m^2/g)
t	Time min
V	Volume of solution (L)
V_{me}	Mesopore volume (cm^3/g)
V_{mi}	Micropore volume (cm^3/g)
V_t	Total pore volume (cm^3/g)
W_f	Final weight of the product (g)
W_o	Initial weight of the raw material (g)
λ_{max}	Maximum wavelength (nm)
SAS	Steam-activated sawdust
CAC	Commercial activated carbon
ICP-MS	Inductively coupled plasma mass spectrometry
FT-IR	Fourier transform infrared spectroscopy
SEM	Scanning electron microscope
XRD	X-ray diffractometer
BET	Brunaeur–Emmett–Teller

INTRODUCTION

The growth and diversity of industrial activities have contributed massively to the development and economic progress of the countries. Unfortunately, this development is almost always accompanied by an immense degradation of the ecosystems via the generation and discharge of different types of pollutants (McKay 1984; Woo-seok 2017). Pollutants, such as heavy metals (e.g., cadmium (Cd), lead (Pb), chromium (Cr), and mercury (Hg)) and phenol, are widely discharged in the wastewater from industries. Some of these heavy metals are carcinogenic. It is, therefore, necessary to remove heavy metals and phenol from wastewater to comply with the regulations pertaining to the environment and human health (McKay 1984; Carvalho *et al.* 2007). Several technologies are developed for the treatment and purification of wastewater including chemical precipitation, oxidation, reduction, solvent extraction, electrolytic extraction, reverse osmosis, ion-exchange, dilution, and adsorption. Among such treatment methods, the adsorption process is found to be the most suitable technique to remove pollutants from wastewater (McKay 1984; Carvalho *et al.* 2007; Qiu & Zheng 2007). It is preferred mostly due to its simplicity, high-efficiency characteristics, design flexibility, technological maturity, and ability to regenerate the exhausted adsorbents. The efficiency of adsorption depends on the type of the adsorbent used, the nature of the solution to be treated, the molecular size of the solute, and the polarity of the contaminant (McKay 1984; Carvalho *et al.* 2007). The wastewater treatment using adsorbents prepared from agricultural waste is technically feasible. Mckay (1984) and Carvalho *et al.* (2007) utilized activated carbon (AC) to adsorb contaminants from wastewater. Some other studies have reported the use of zeolites in wastewater treatment (Elboughdiri 2020). In addition, synthetic polymeric and silica-based materials have also been reported as adsorbents (Mojoudi *et al.*

2019). AC is the most widely used adsorbent for the removal of various types of metals. Nevertheless, the application of AC is not feasible due to its high price and the cost associated with the regeneration of the spent adsorbent that is significantly lost during the purification process (Ngah & Hanafiah 2008; Caetano *et al.* 2009; Lütke *et al.* 2019).

Several natural products have shown an ability to selectively bind molecules from aqueous solutions. Among these products, sawdust is of great interest in terms of the heavy metal and phenol removal efficiency. It is considered as a promising tool for the treatment of contaminated effluents due to its abundant availability and the requirement of little processing (Ajmal *et al.* 1996; Srivastava *et al.* 2006; Ngah & Hanafiah 2008).

Most research studies reported in literature encompass the batch adsorption of single-component aqueous solutions that is not valid for a multicomponent system (Ajmal *et al.* 1996; Srivastava *et al.* 2006; Omprakash *et al.* 2017). The sorption capacities calculated from the batch mode are useful in providing information about the effectiveness of the adsorbate–adsorbent system only (Liyana-Pathirana & Shahidi 2005; Witek-Krowiak 2013). The present work focuses on the use of adsorbents prepared from sawdust to study the co-adsorption of Cr^{3+}, Zn^{2+}, Pb^{2+}, and phenol from industrial wastewater. The kinetic model and equilibrium parameters are determined to understand the mechanism of adsorption, and the cost of production of the steam-activated sawdust (SAS) adsorbent is estimated and compared to the commercial AC (CAC).

MATERIALS AND METHODS

Materials

Stock solutions of Cr, Zn, Pb, and phenol were prepared by using chemical products supplied by Karl Fischer®. Nitrogen (N_2) gas, supplied by AIR LIQUIDE® (Tunisia), was employed during the preparation of AC from sawdust. Dilute HCl and NaOH were utilized for pH adjustment. All synthetic solutions were prepared using distilled water. The adsorbents were derived from pine sawdust, thanks to their availability and desirable physical characteristics.

Equipment

The heavy metal ion concentrations were determined using the ICP-MS (Agilent, 7500). For all the samples, the phenol levels were quantified using the UV–VIS (Shimadzu, 1800) at a fixed wavelength ($\lambda_{max} = 269.0$ nm) utilizing cuvettes of quartz.

An oven (Memmert, UN30) was utilized for heating the samples (until 250 °C) and drying purposes. Nevertheless, if higher temperatures were needed, a muffle furnace (*FALC, FM 8.2*) was used. An incubator with a shaking platform (Thermo Scientific, 222000) was utilized to mix the adsorbate–adsorbent suspensions throughout batch adsorption tests. The pH level was determined utilizing a pH-meter (Hanna Instruments, HI-991003).

The AC from sawdust was prepared in a fluidized-bed reactor (FBR). A regulated peristaltic pump was employed to adjust the water flow into the device and to furnish the used water feed into the adsorption column. Furthermore, the X-ray diffractometer (XRD; Thermo Scientific, ARL™ X'TRA), Fourier transform infrared spectroscopy (FT-IR) (Bruker, ALPHA II), and scanning electron microscope (SEM; Keysight Techologie, U9320A 8500) were used to characterize the adsorbents used.

Preparation and characterization of adsorbents

The adsorbent efficiency is influenced by the particle size. For the sake of precision and consistency, the particle sizes of the adsorbents need to be identical. A size range of 53–180 μm is used for the adsorbents studied. The identification of the adsorbents is made by the evaluation of functional groups, phases, surface morphology, specific surface area, and pore structural indicators.

The X-ray diffraction spectrum is obtained using an XRD with radiation at 40 kV and 50 mA to determine the presence of phases. Fourier transform infrared (FT-IR) spectra of the adsorbents are recorded in the range of 500–4,000 cm^{-1} to explore the number and positions of the functional groups available for the binding of the adsorbate. The surface morphology of the adsorbents is visualized in a SEM operated at the accelerating voltage of 20 keV. The Brunaeur–Emmett–Teller (BET) surface area (S_{BET}) and pore structural indicators of the adsorbents are evaluated

from the adsorption–desorption isotherm of N_2 at 77 K employing the Micrometrics Surface Area and the Porosity Analyzer.

Steam-activated sawdust

The sawdust was washed three times with distilled water. This was followed by drying the sawdust in an oven at 120 °C for 24 h to remove the moisture content and organic impurities. It was pulverized and sieved to a particle size range of 53–180 μm. For the carbonization step, 150 g of sawdust was fed into the FBR that was preheated to 600 °C for 1 h and purged with N_2 gas. The resulting product was removed from the reactor and allowed to cool in a desiccator. The carbonized sawdust was fed into the reactor under N_2 flow and activated at 800 °C for 1 h. The AC thus obtained was designated as SAS that was kept in a desiccator for adsorption tests.

Commercial AC

Extruded AC pellet (C270-186121) is used extensively in the chemical and pharmaceutical industries. For the comparison of adsorption efficiency, the extruded AC pallet was purchased from Thermo Fisher Scientific®. This CAC adsorbent (particle size = 53–180 μm) results in a very small hydrodynamic pressure drop in liquid-phase applications.

Simulated wastewater preparation

The wastewater solutions of Cr, Zn, Pb, and phenol (1,000 mg/L) were prepared and diluted with distilled water to achieve the pollutant concentrations in synchrony with the concentrations of the usual industrial wastewater reported in the literature. These concentrations range from 20 to 200 mg/L for phenol and 0.1 to 100 mg/L for heavy metals (Cr, Zn, and Pb) (Iglesias-Carres *et al.* 2019). The pH of the solutions was regulated by HCl or NaOH (0.2 M).

Adsorption experiments

Batch adsorption experiments were conducted to determine the optimum adsorbent weight, equilibrium time, adsorption kinetics, and adsorption isotherm. For the adsorption experiments, the initial concentrations of the adsorbate were determined, and the blank solutions were utilized to check if there was any adsorption on the surface of the conical flask. The data acquired from the kinetic adsorption trials were employed to estimate the adsorption capacity, q_e (mg/g), using the following equation:

$$q_e = (C_o - C_e) \times \frac{V}{m} \quad (1)$$

where C_o and C_e are the preliminary and equilibrium adsorbate concentrations (mg/L), respectively, V is the volume of industrial wastewater (L), and m is the weight of adsorbent (g).

Equilibrium and kinetic studies were conducted in a fixed-bed column (Pyrex glass, I.D. = 2.5 cm, $L = 45$ cm) at ambient temperature. The tests were performed in a downflow mode that guarantees that the bed stays well packed throughout the experiment and a maximum contact between the adsorbent and the adsorbate prevails. A constant volumetric flow rate, pH, and the initial concentration of the simulated wastewater feed were maintained throughout the experiment.

Optimum adsorbent weight

The optimum weights for treating the industrial wastewater utilizing SAS and CAC were evaluated by changing the adsorbent mass from 0.2 to 4.0 g under the chosen residence time (48 h) at a pH value of 4.0 by employing contaminated water constituted of 50 mg/L of the heavy metal ions and 110 mg/L of phenol. The chosen agitation velocity and temperature for the trial runs were 250 rpm and 25 °C, respectively. The percentage reduction of metal ions from the aqueous solution was evaluated by utilizing the following equation:

$$P_r(\%) = \frac{(C_o - C_e)}{C_o} \times 100 \quad (2)$$

Equilibrium and kinetic studies

The equilibrium adsorption isotherm data were generated by making a fixed predetermined optimum weight of adsorbent

(SAS or CAC) contact with 100 mL of industrial wastewater with the concentration of metal ions and phenol ranging from 20 to 90 mg/L at a pH value of 4.0 in 250 mL Erlenmeyer flasks. The flasks were agitated at 250 rpm at 25 °C for a predetermined contact time. At the end of the experiment, the residual concentrations of the metal ions and phenol were measured. The equilibrium adsorption capacity (q_e) values were calculated using Equation (1), and the experimental results were fitted to the adsorption isotherms.

For kinetic studies, a predetermined optimum weight of the adsorbent was made to contact with 100 mL of simulated wastewater consisting of 50 mg/L of the heavy metal ions and 110 mg/L of phenol at a pH value of 4.0 and agitated at 250 rpm at 25 °C. At different intervals of time, 0.5 mL of solutions were withdrawn and analyzed. The adsorption capacity at time t (q_t, mg/g) was calculated using the following equation:

$$q_t = (C_o - C_t) \times \frac{V}{m} \quad (3)$$

where C_t (mg/L) is the residual concentration at time t.

RESULTS AND DISCUSSION

The efficiency of the adsorbents is juxtaposed, and an attempt is made to correlate the physicochemical properties of adsorbents with their efficiency. Moreover, the adsorption findings for eliminating heavy metals and phenol utilizing SAS and CAC are presented and interpreted. Since only limited data are available on the kinetics of Cr reduction by sawdust-based adsorbents, estimates of the maximum adsorption capacity are made from the Langmuir isotherm model to show the adsorption kinetic modeling of Cr for the two adsorbents. This decision was taken because there are restricted references on the kinetics of Cr reduction employing adsorbents extracted from sawdust.

Characterization of the SAS

Figure 1 illustrates the X-ray diffraction of the SAS. It shows that SAS is amorphous and may contain carbon and graphite.

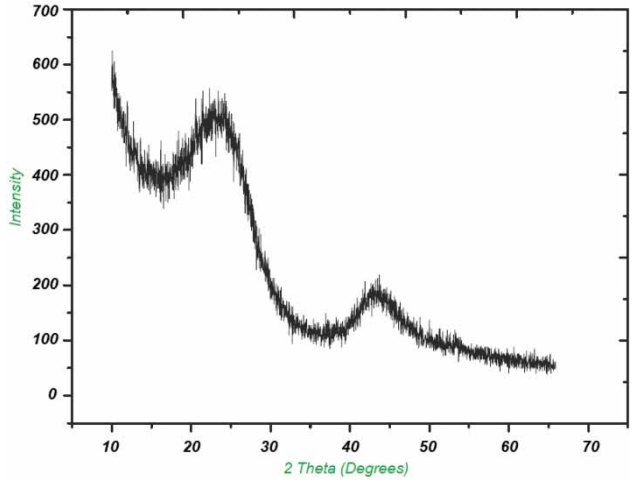

Figure 1 | The X-ray diffraction profile of SAS.

The FT-IR spectrum of SAS before and after adsorption is presented in Figure 2. The peak positions show major absorption bands at 2,656, 2,089, 1,997, 1,841, 1,561, 1,215, 947, and 669 cm^{-1}. The band at 2,669 cm^{-1} is likely to represent the O–H stretching in carboxylic acids. The peak at 2,089 cm^{-1} represents the C–C stretching in alkynes, and the peak at 1,561 cm^{-1} is the characteristic peak for C=O in the Quinone structure (Elboughdiri 2018a). The band at 1,215 cm^{-1} is due to C–H deformation vibration. The peak at 669.3 cm^{-1} can be assigned to the out-of-plane C–H bending mode of an aromatic compound (Al-Qodah & Shawabkah 2009). Following the adsorption

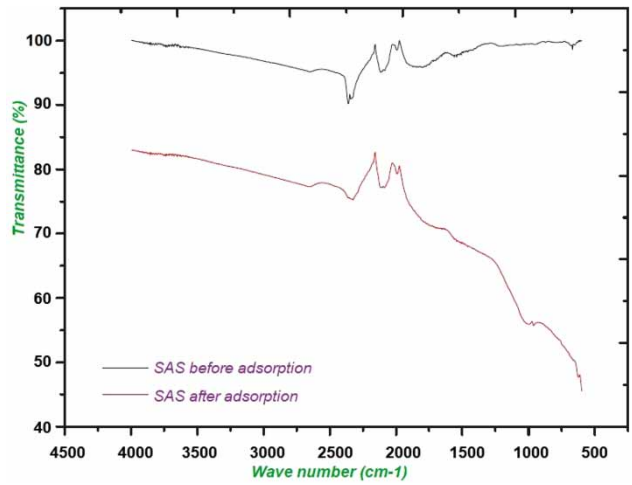

Figure 2 | FT-IR spectra of SAS before and after the adsorption of heavy metals and phenol.

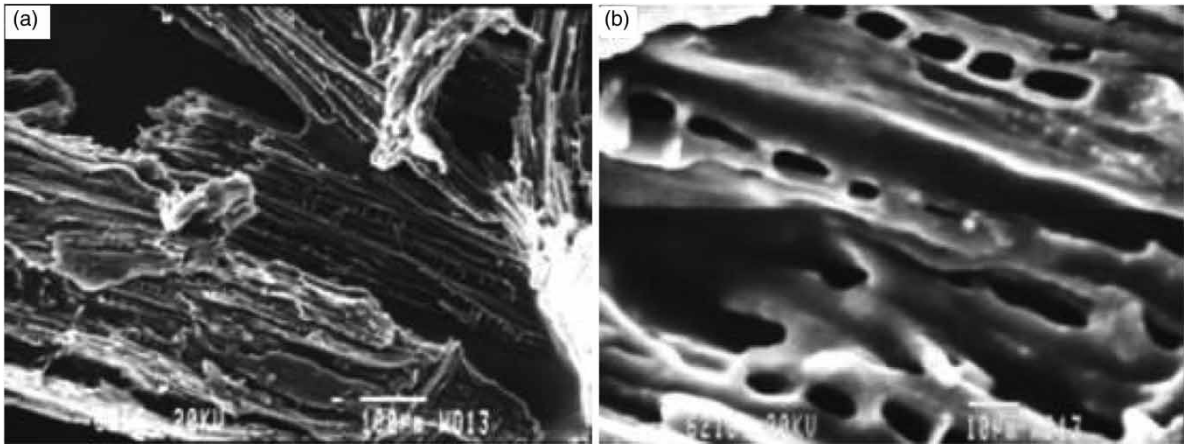

Figure 3 | SEM micrographs of SAS before adsorption at 140× (a) and 1,200× (b) magnification.

of heavy metals and phenol, the bands at 2,656, 2,363, 1,842, 1,561, 947, and 669 shifts to 2,899, 2,604, 1,749, 1,522, 1,016, and 629 cm^{-1}, respectively. All such results propose chemical fixation of heavy metals and phenol onto SAS.

The changes seen in the intensity and positions of peaks (Figure 2) indicate that heavy metals (Cr, Zn, and Pb) and phenol create functional groups that are available on SAS complexes. Such modifications confirm that the adsorption process has occurred. Also, the shift in wave numbers corresponds to changes in the energy of the functional groups, suggesting the involvement of carboxyl, hydroxyl in the binding of heavy metals, and the formation of complexes. Similar observations were observed in the heavy metal removal using SAS and other adsorbents (Al-Omair & El-Sharkawy 2007; Wiwid *et al.* 2014; Banerjee *et al.* 2016; Solgi *et al.* 2017).

Figure 3 represents SEM images at different magnifications. It shows that the external surface of SAS is filled with cavities that emerge due to the evolution of volatile compounds throughout the carbonization step. Identical results are reported by Mohanty *et al.* (2005) for the morphological properties of AC fabricated from sawdust.

Characterization of the CAC

Figure 4 represents the XRD spectrum of CAC. It shows that AC can be defined as an amorphous form of graphite with a random structure of graphite plate showing a highly porous structure with a set of cracks and crevices on the molecular level. Juxtaposing the XRD sample of CAC with different

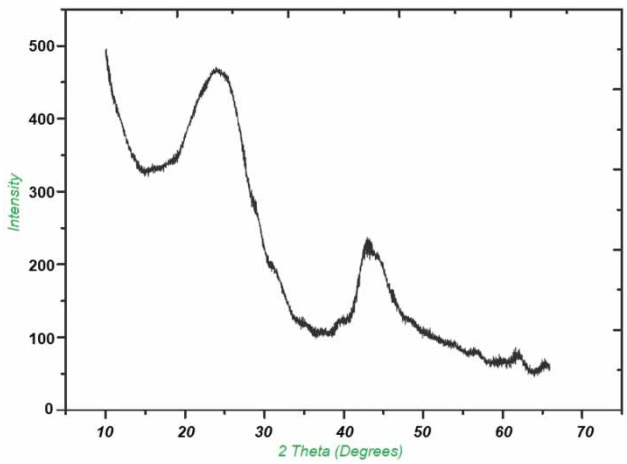

Figure 4 | The X-ray diffraction profile of CAC.

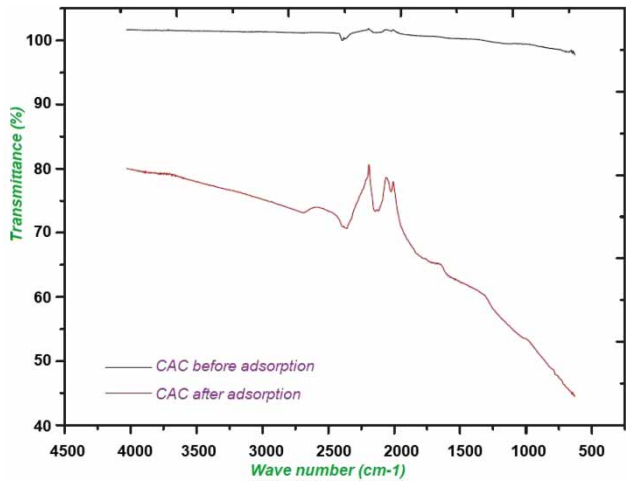

Figure 5 | FT-IR spectra of CAC before and after the adsorption of heavy metals and phenol.

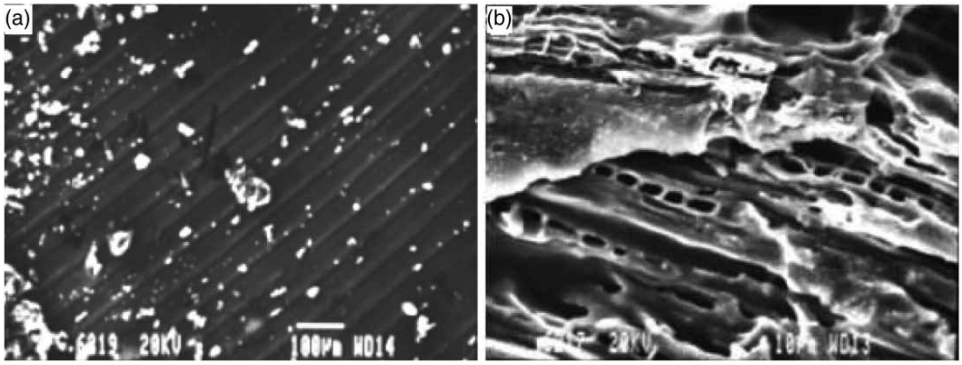

Figure 6 | SEM images of CAC before adsorption at 140× (a) and 600× (b) magnification.

adsorbents indicates that the intensity of the peak about 42.3° that represents graphite follows the order: CAC > SAS. In addition, the intensity of the peak about 24.4° because of carbon in the adsorbents follows the order: SAS > CAC.

Figure 5 illustrates the FT-IR spectra of CAC before and after the adsorption. Juxtaposing the FT-IR spectra of CAC and SAS before adsorption shows that the intensity of the peaks on the spectra of CAC is smaller than SAS. Moreover, the adsorbents possess frequent functional groups that are C–H in aromatic and aliphatic compounds, C=O in the Quinone structure, carbonyl groups in aldehydes and ketones, C–O groups, alkyl groups, and the O–H groups in the carboxylic acids.

The SEM micrograph in Figure 6 is very much comparable to that of SAS that shows a heterogeneous phase material. The CAC possesses a honey comb-like structure that is highly porous (Figure 6).

Surface area and porosity of the adsorbents

The surface features of the adsorbents (Table 1) show that the surface area of SAS is within the range of CAC surface area (500–1,500 m^2/g). Consequently, their efficiency is anticipated to be identical to that of CAC (ElHajam *et al.* 2020).

Table 1 | Surface features and pore structure of the SAS and CAC

Adsorbent	S_{BET} (m^2/g)	S_{mi} (m^2/g)	V_t (cm^3/g)	V_{mi} (cm^3/g)	V_{me} (cm^3/g)	V_{mi}/V_t
SAS	795.68	588.80	0.386	0.258	0.128	0.668
CAC	1,057.04	785.68	0.584	0.387	0.197	0.663

S_{BET}, Brunaeur–Emmett–Teller (BET) surface area (m^2/g); S_{mi}, micropore-specific area (m^2/g); V_t, total pore volume (cm^3/g) ; V_{mi}, micropore volume (cm^3/g); V_{me}, mesopore volume (cm^3/g); V_{mi}/V_t, micropore volume and total pore volume ratio.

Optimum adsorbent mass

Figure 7 indicates that the percentage elimination of Cr, Zn, Pb, and phenol augments with an increasing adsorbent weight. Increasing the amount of adsorbent results in an elevation in the number of active surface sites for adsorption (Goel *et al.* 2005). The highest efficiency of the heavy metal and phenol removal is observed at an optimum weight of 2.0 and 1.8 g for SAS and CAC, respectively.

Kinetic studies

The observed order of residence time can be related to the specific surface area of the adsorbents, and the rapid kinetics has significant practical importance ensuring efficiency (Elboughdiri 2018b). The experimental results of the effect of contact time on the batch adsorption of heavy metals and phenol at an initial pH value of 4.0 at 25 °C are presented in Figure 8. The initial rapid adsorption paves the way to a very slow approach to equilibrium. The contact time selected was 4 h for the removal of heavy metals and phenol using SAS and CAC.

Adsorption kinetic modeling

Several models are applied to evaluate the experimental information related to the adsorption mechanism. Pseudo-first-order, pseudo-second-order, and the Weber–Morris kinetic models were tried to determine the kinetic indicators and the adsorption route (Bingxin *et al.* 2020). To define the equilibrium isotherms, the experimental information of

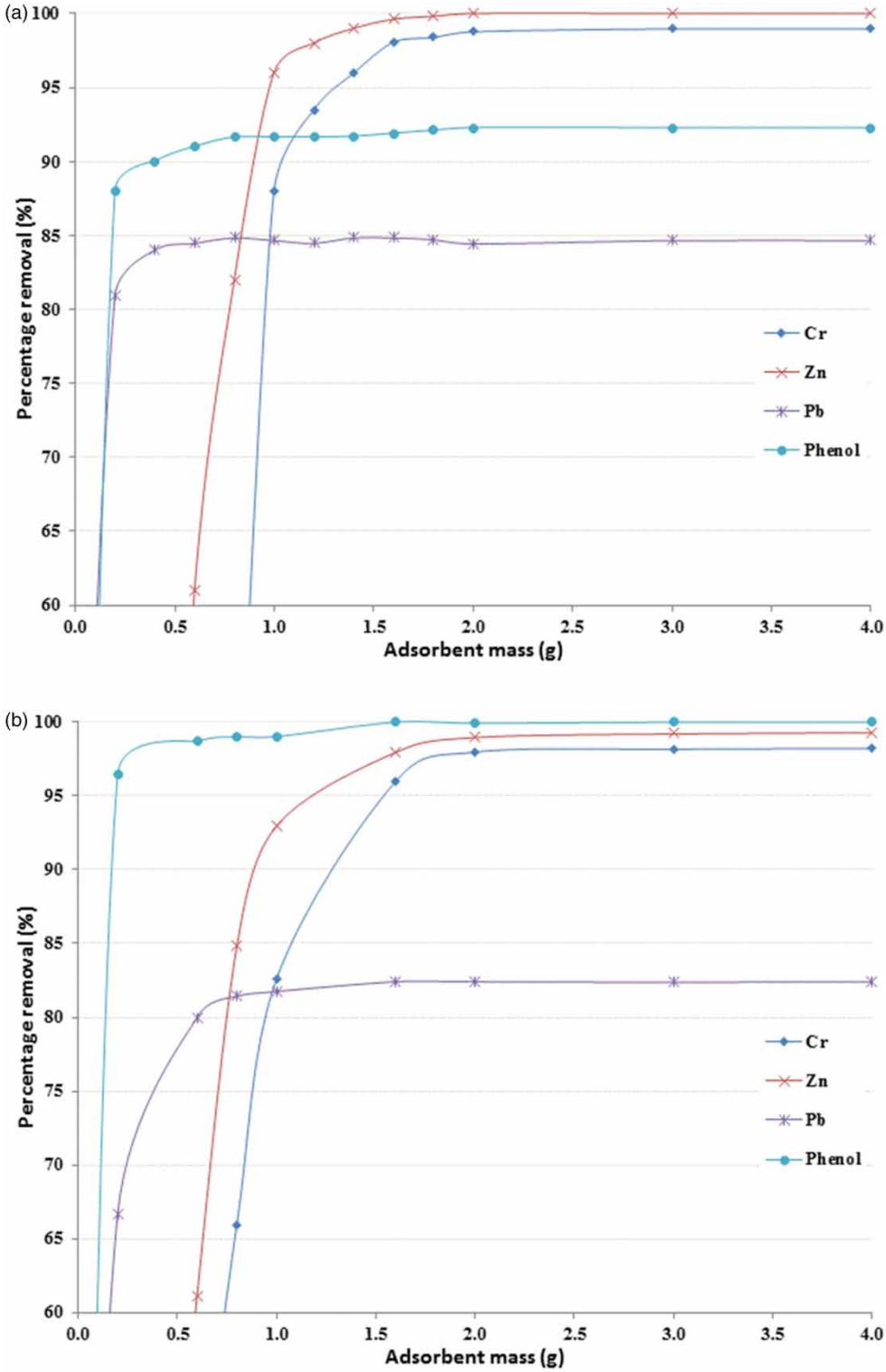

Figure 7 | Removal of heavy metals and phenol using SAS (a) and CAC (b) at pH = 4.0, temperature = 25 °C, shaking speed = 250 rpm, contact time = 48 h, initial metal concentration = 50 mg/L, initial phenol concentration = 110 mg/L.

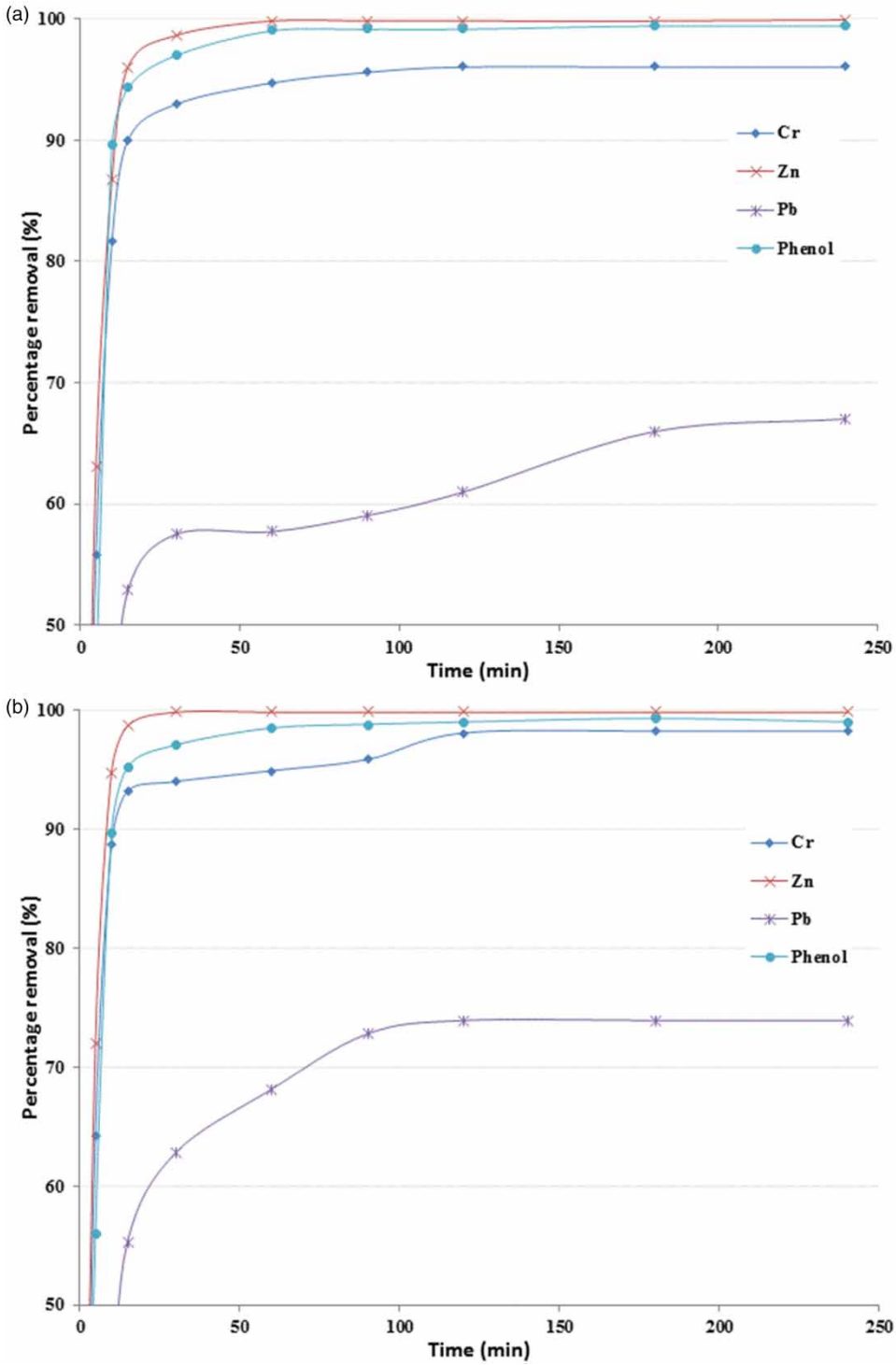

Figure 8 | Data for determining contact time using SAS (a) and CAC (b) for the treatment of industrial wastewater.

the removal of Cr, Zn, Pb, and phenol is discussed using the Langmuir and Freundlich isotherm models. The findings are shown in Figure 9(a)–9(c).

The evaluated equilibrium adsorption capacity (q_e) estimates and coefficients linked to the pseudo-first-order and pseudo-second-order kinetic plots are given in Table 2.

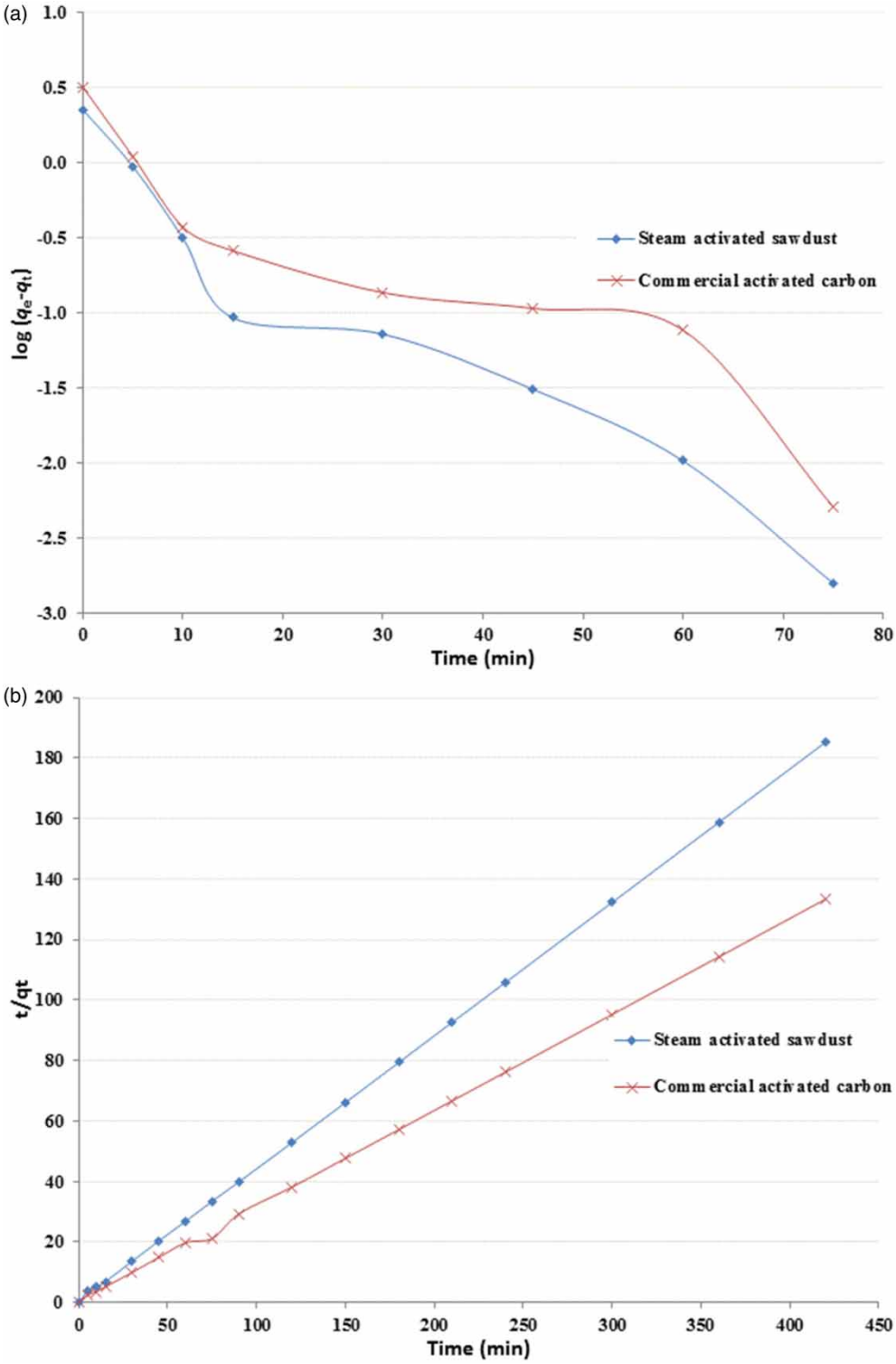

Figure 9 | (a) Lagergren pseudo-first-order plots for Cr adsorption on SAS and CAC. (b) Pseudo-second-order plots for Cr adsorption on SAS and CAC. (c) Weber and Morris intraparticle diffusion plots for Cr adsorption on SAS and CAC. *(Continued.)*

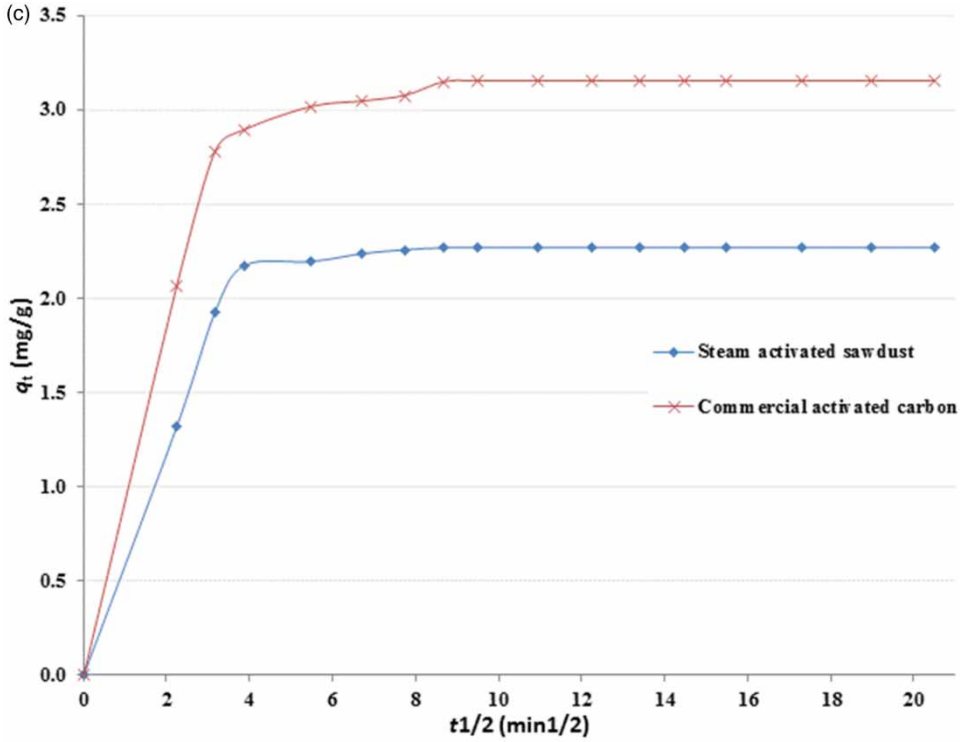

Figure 9 | Continued.

Table 2 | Kinetic parameters for Cr adsorption

Model	Parameter	SAS	CAC
Pseudo-first-order	k_{ad} (min^{-1})	0.0507	0.0392
	q_e (mg/g)	1.0544	1.6673
	R^2	0.8170	0.8340
Pseudo-second-order	k_2 ($g{\cdot}mg^{-1}$ min^{-1})	0.3126	0.1934
	q_e (mg/g)	2.2883	3.1746
	R^2	0.9999	0.9999
/	Experimental q_e (mg/g)	2.1650	3.0256

The correlation coefficients (R^2) are 0.817 and 0.834 for the pseudo-first-order and pseudo-second-order, respectively. Furthermore, the q_e values anticipated by the pseudo-first-order model are not in agreement with the practical estimates that suggest that Cr adsorption did not satisfy the pseudo-first-order model. Moreover, the R^2 value for the pseudo-second-order model is 0.9999, and the anticipated q_e estimates agreed well with the practical findings.

The results indicate that the pseudo-second-order kinetic model fits well with the kinetics adsorption process for SAS and CAC that makes it better than the pseudo-first-order kinetic model.

Figure 9(c) presents the multilinear plots of the adsorbed chromium ion mass per unit mass of adsorbent versus $t^{1/2}$ for SAS and CAC. The initial time period is attributed to the diffusion of Cr through the solution to the external surface of the adsorbent. This is followed by the first linear portion that describes the gradual adsorption stage, where the intraparticle diffusion is rate-limiting. The second linear portion is attributed to the final equilibrium stage, where intraparticle diffusion starts to slow down due to the lower concentration of Cr in the solution (Alzaydien 2009; RuiYan *et al.* 2019; Sumon *et al.* 2020). The slope of the first linear portion characterizes the rate parameter corresponding to the intraparticle diffusion.

The data presented in Table 3 show that the adsorption rate is higher in the first stage (k_{id1}) as compared to the

Table 3 | Intraparticle diffusion constants for Cr adsorption

Adsorbent	Parameter k_{id1} (mg/g min)	R_1^2	k_{id2} (mg/g min)	R_2^2
SAS	0.575	0.995	0.008	0.815
CAC	0.886	0.998	0.020	0.842

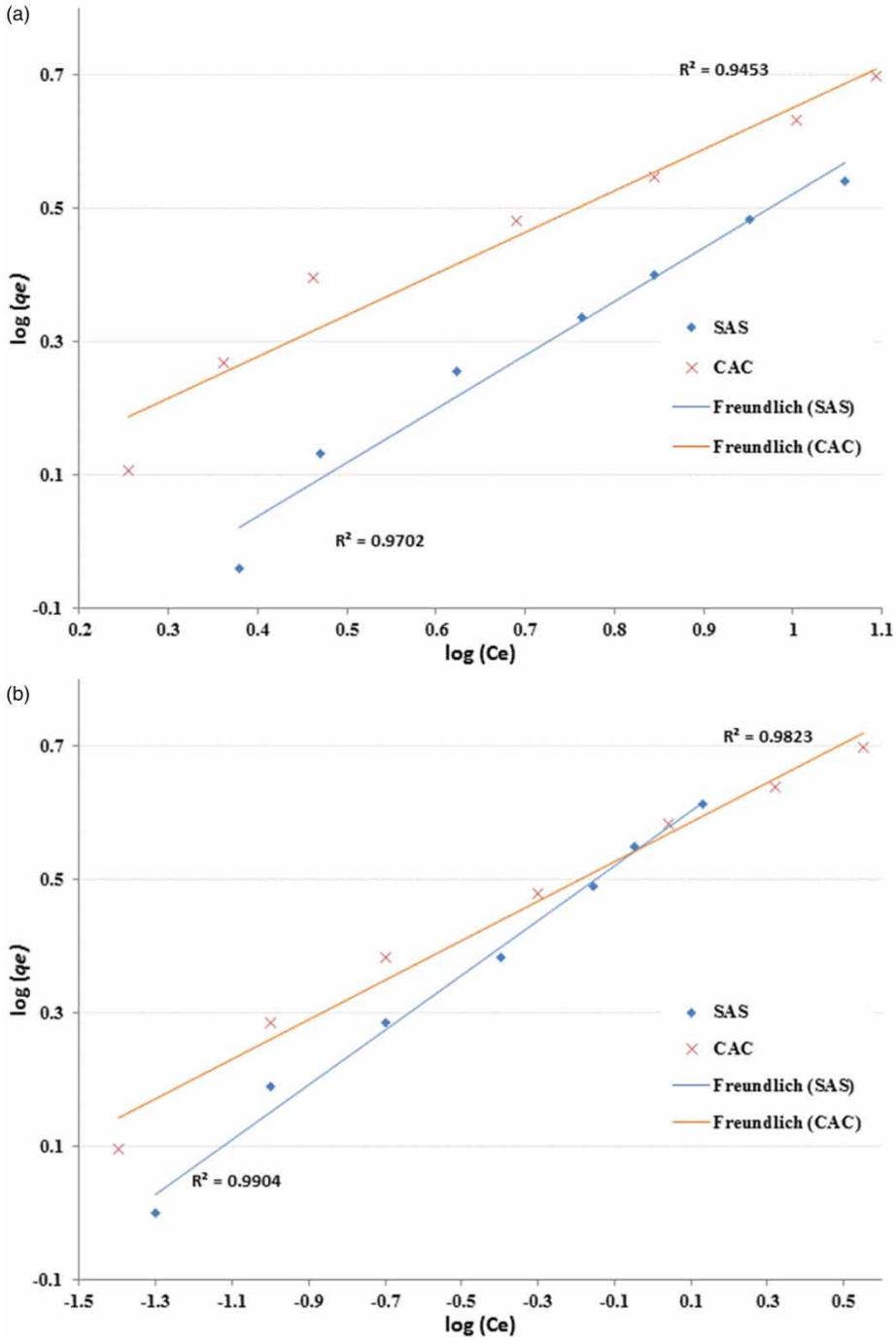

Figure 10 | Fitting curves of adsorption for Cr (a), Zn (b), Pb (c), and phenol (d) removal using SAS and CAC through the Freundlich model. *(Continued.)*

second stage (k_{id2}). In the beginning, Cr is adsorbed by the external surface of the adsorbent particles. Therefore, the sorption rate is significantly elevated. When the external surface saturates, Cr^{3+} starts to diffuse deep inside the pores of the adsorbent particles. At this stage, the diffusion resistance increases, and therefore the diffusion rate decreases. Due to the decrease of the chromium ion concentration in the solution, the diffusion rate gets lower. Therefore, the changes

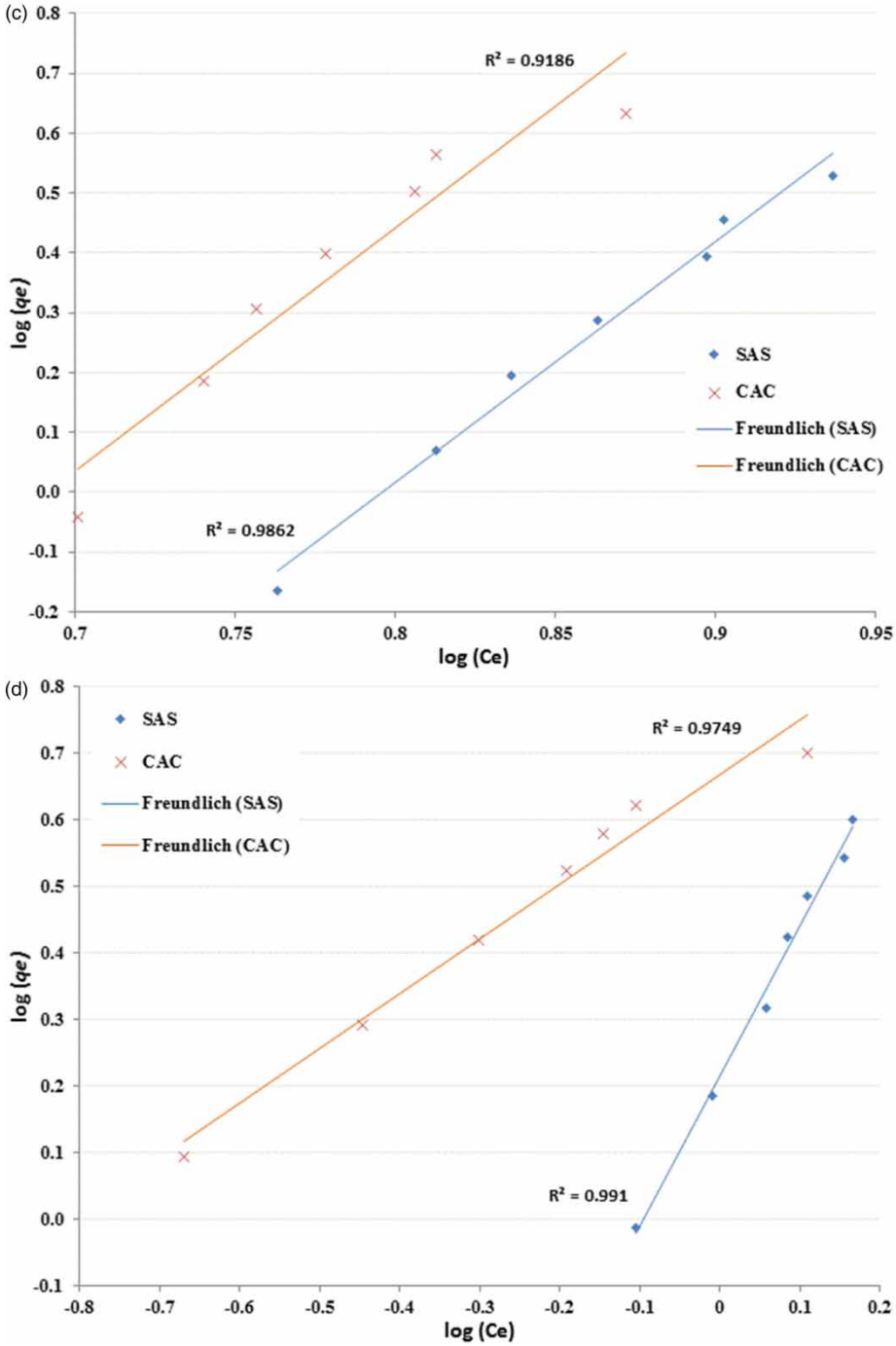

Figure 10 | Continued.

in k_{id1} and k_{id2} may be attributed to the adsorption stages of the external and internal surfaces and the equilibrium approach. Similar phenomena are reported by Sun & Yang (2003).

Equilibrium modeling

The numerical values of the results of industrial wastewater treatment utilizing SAS and CAC were fitted to the

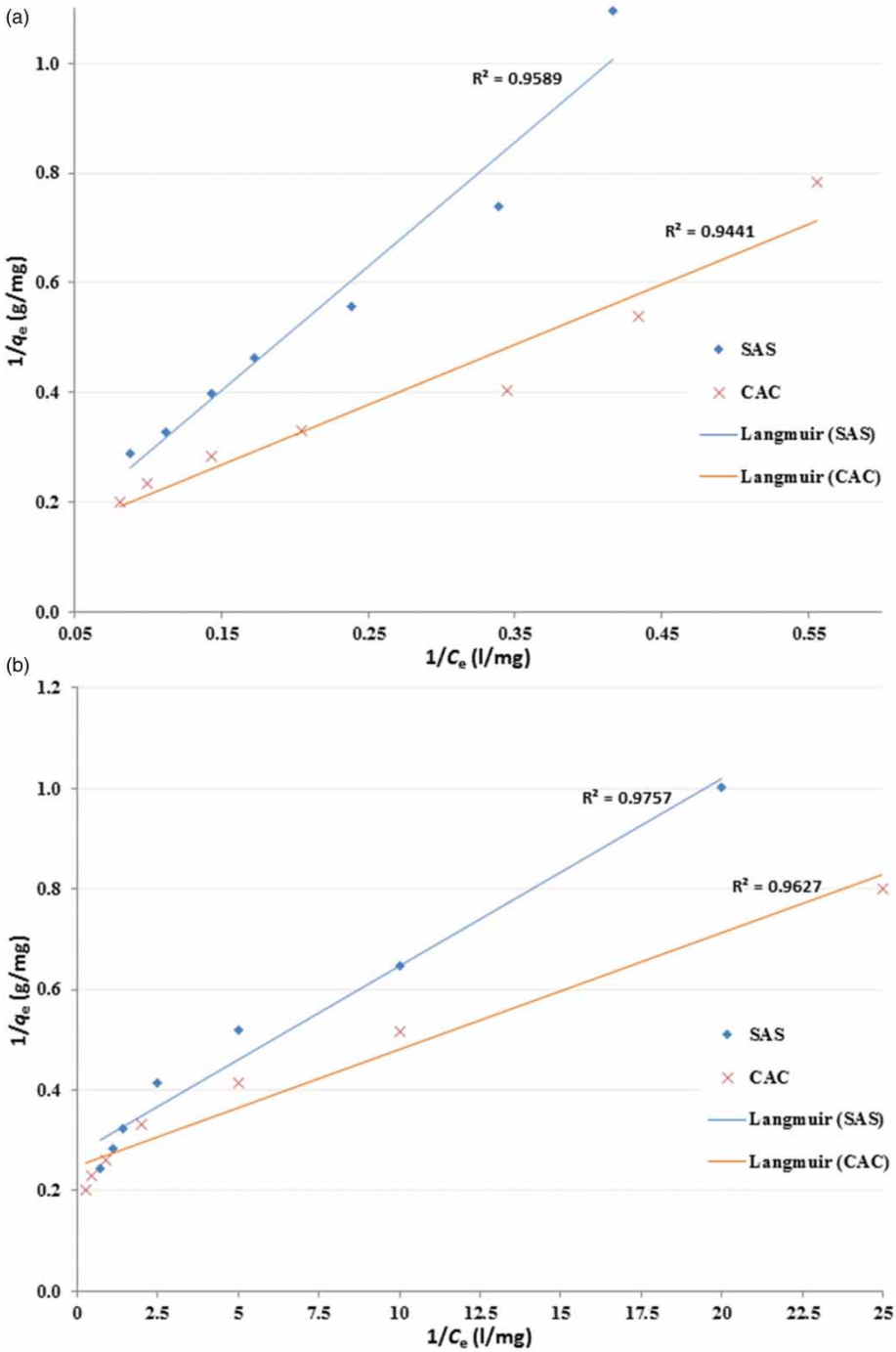

Figure 11 | Fitting curves of adsorption for Cr (a), Zn (b), Pb (c), and phenol (d) removal using SAS and CAC through the Langmuir model. *(Continued.)*

Langmuir and Freundlich model. The findings are presented in Figures 10 and 11, respectively.

If juxtaposed to the Langmuir isotherm, it is observed that the Freundlich isotherm resulted in an excellent fit with the experimental data for all heavy metals and phenol.

The empirical parameters for both isotherms are presented in Table 4. The sequence of sorption affinity for both SAS and CAC is such that: Cr > Zn > Pb. This similarity in the sequence of sorption affinity can be explained by the fact that both CAC and SAS have almost similar physicochemical

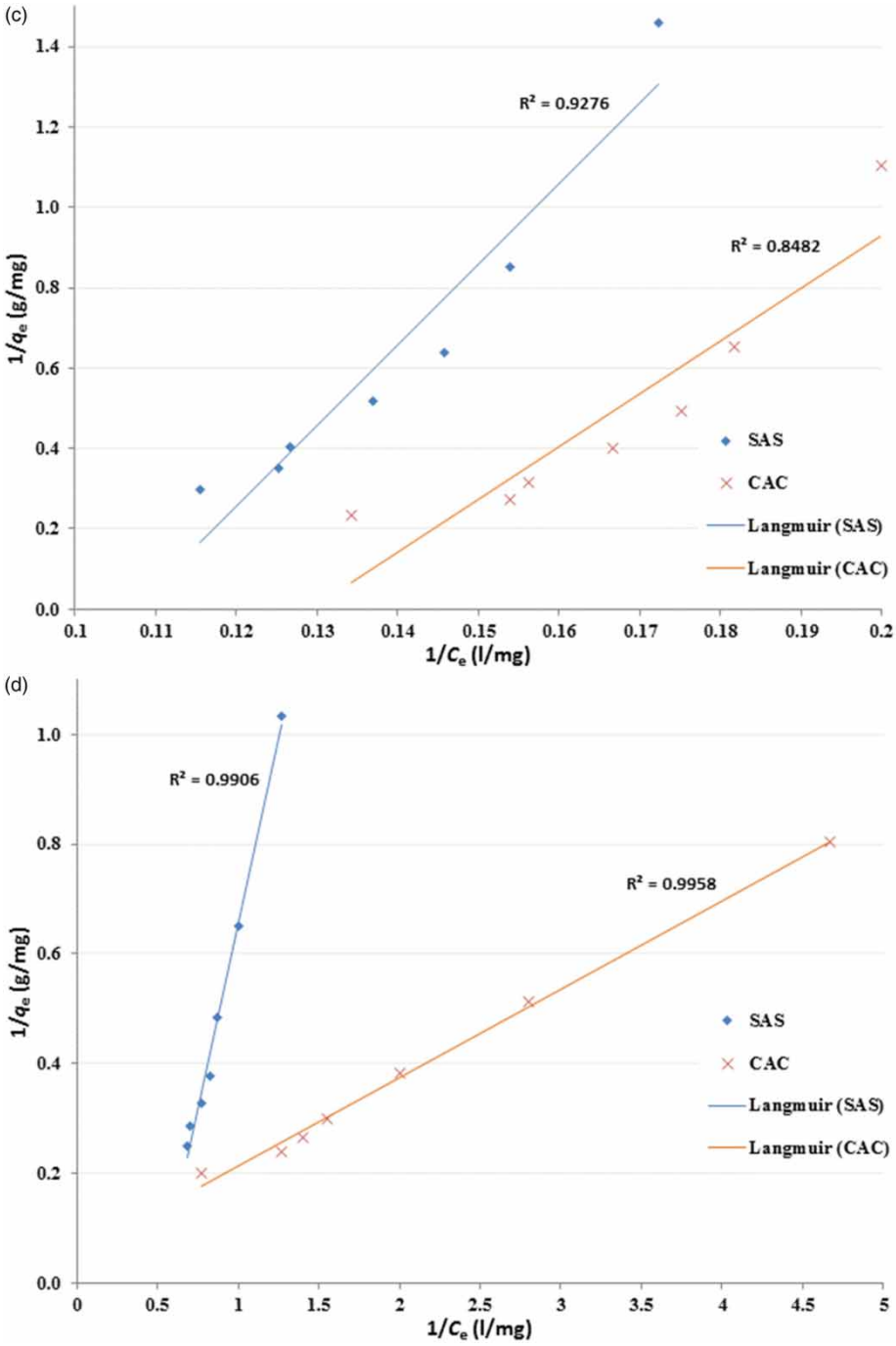

Figure 11 | Continued.

properties. The q_{max} values show that the order for Cr-binding affinity is such that: CAC > SAS, which agrees with the q_e values calculated from the pseudo-second-order model.

The removal of phenol by CAC and SAS is better described by the Langmuir isotherm. The experimental data deviate more in the case of the Freundlich model than the Langmuir model (Figures 10(d) and 11(d)) for the studied adsorbents. This is indicated by the regression coefficient (R^2) values of the linear plots. The sequence of sorption affinity for phenol is in accordance with the

Table 4 | Freundlich and Langmuir isotherm constants for industrial wastewater using SAS and CAC

		Langmuir			Freundlich		
Adsorbate	**Adsorbent**	q_{max} (mg/g)	K_L (L/mg)	R^2	n	K_F (mg/g)	R^2
Chromium	SAS	9.524	0.096	0.9589	1.244	0.520	0.9702
	CAC	15.39	0.028	0.9441	1.603	1.062	0.9453
Zinc	SAS	4.016	10.826	0.9757	2.439	3.639	0.9904
	CAC	5.435	0.240	0.9627	3.378	3.606	0.9823
Lead	SAS	0.464	0.107	0.9276	0.249	0.0006	0.9862
	CAC	0.591	0.129	0.8482	0.193	0.0003	0.9186
Phenol	SAS	10.000	0.003	0.9906	0.438	1.622	0.991
	CAC	19.600	0.317	0.9958	1.214	4.645	0.9749

increase in the surface area of the adsorbents with CAC having the highest and SAS having the lowest surface area.

Cost analysis

Costs were developed assuming a 79% yield of SAS (158 g output), 320 days/year of production, for 24 h/day at $10 per h (Tables 5 and 6). The production of SAS requires a fixed capital investment of $1.575 (Table 5) and an operating cost of $6.678 (Table 6). The estimation of the equipment purchase cost was determined following McMaster-CARR (McMaster-CARR) and McGraw Hill (McGraw Hill) websites.

Table 5 | Estimation of the purchased equipment cost for SAS production and the cost of their usage for 3 h

Equipment	**Capacity**	**Cost ($)**	**Working cost for 3 h ($)**
N_2 cylinder	8 L/min	200	0.008
Rotameter	50 L/min	300	0.012
Beakers	2 × 250 mL, 2 × 500 mL	40	0.016
Peristaltic pump	5.41 g/min	150	0.006
Temperature controller	100–1,000 °C	200	0.008
Electric furnace	600 °C	2,000	0.078
FBR	2 L	15,000	0.586
Thermocouple	100–1,000 °C	50	0.002
Acetone	2.5 L	90	0.800
Sieve	20–200 µm	150	0.006
Balance	2.5 kg	700	0.027
Muffle furnace	20–180 °C	600	0.023
Desiccator	0.5 L	100	0.004
Total			1.575

Table 6 | The operating costs for SAS

Item	**Capacity/description**	**Cost ($)**
Raw materials *(Sawdust)*	200 g	0.003
Utilities *(Steam, water, electricity)*	1 kg of steam, 1 L of water, 0.3 MWh of electricity	2.500
Labor *(Operating labor, maintenance labor)*	One technician for 15 min	2.500
Supplies *(Operating supplies, maintenance supplies)*	One technician of maintenance for 1 h/month	0.014
General works *(General and administrative)*	One administrator for 10 min	1.670
Total		6.687

The operating costs for labor, supplies, and general works are based on percentages given in Peters and Timmerhaus (cited in Ng *et al.* 2003; Lima *et al.* 2008).

The total fixed capital investment was estimated and presented in Table 7 by assuming the economic life of 10 years for all equipment and 1 year for the laboratory glassware. Capital costs were estimated on percentages of the total equipment cost according to Peters and Timmerhaus (cited in Ng *et al.* 2003; Lima *et al.* 2008).

Table 7 shows that the estimated cost for SAS is $52 per kg. The cost of CAC is $80–300 per kg (Indiamart). This production cost concerns the industrial sector and has a great variation based on plant's size and location plant, which affects the energy consumption and other production

Table 7 | Summary of costs for SAS

	Source	Cost ($)
Purchased equipment cost	From Table 5	1.575
Capital cost	From Table 5	0.001
Total fixed capital investment	Purchased equipment cost plus capital cost	1.576
Total operating cost	From Table 6	6.687
Estimated production of SAS	158 g produced in 3 h	–
Estimated cost for steam-activated sawdust production per kg	Total fixed capital investment plus total operating cost) dived by the estimated production of SAS	52.297

utilities. Therefore, it is still higher than the estimated laboratory production cost.

CONCLUSION

In this study, the SAS adsorbent is successfully prepared, and its efficiency for the removal of recalcitrant compounds from industrial wastewater is juxtaposed to the CAC adsorbent.

From the data of the present investigation, the following can be concluded:

- The discharge of industrial wastewater from numerous industries is almost inevitable. Our findings can assist for conceiving and implementing a convenient ecological control plan to reduce the harmful effects of the industrial wastewater.
- The SAS adsorbent has proved to be a promising adsorbent media for the removal of heavy metals and phenol from industrial wastewater.
- The physicochemical properties of SAS and CAC are mostly identical except for the specific surface area.
- The adsorbents' surfaces are complicated because of the existence of various functional groups. Certain functional groups, such as –OH and –COOH that are responsible for cation binding, are detected on the adsorbents' surfaces.
- The maximum monolayer adsorption capacity of the adsorbents corresponds to the specific surface area of the adsorbents. The adsorbents with an elevated specific surface area possess higher maximum monolayer adsorption capacities with a few exceptions. The largest amount (10.0 mg/g) adsorbed by SAS belongs to phenol with Cr on the second largest position (9.5 mg/g).
- Equilibrium data for the metals' removal data satisfy well with the Freundlich isotherm; however, phenol removal data satisfy well with the Langmuir adsorption isotherm model. Additionally, the removal of Cr followed pseudo-second-order kinetics proposing chemisorption because of the sharing of electrons among the adsorbent surface and the orbitals of Cr^{3+} for the tried adsorbents. Intraparticle diffusion is not the only stage dominating the global adsorption method of Cr in the studied adsorbents.
- The effect of several variables, such as pH, temperature, preliminary phenol concentration, and residence time, should be examined. Furthermore, the wanted adsorption circumstances, adsorption kinetics model, and equilibrium model for heavy metals and phenol will be selected.
- The production cost of the CAC adsorbent at the industrial level has a large variation ($80–300 per kg) based on plant's size and location. It stills higher than the estimated laboratory production cost of the SAS adsorbent ($52 per kg).

Additional pretreatment trials would be performed to ameliorate the physicochemical features such as pore volume and adsorption active sites. To enlarge the practicability of the SAS adsorbent, tests need to be accomplished using actual industrial wastewater instead of a synthesized one.

FUNDING

This research has been funded by the Research Deanship of the University of Ha'il, Saudi Arabia, through the project RG-20 101.

CONFLICTS OF INTEREST

The authors declare that they have no known competing financial interests or personal relationships that could have appeared to influence the work reported in this paper.

DATA AVAILABILITY STATEMENT

All relevant data are included in the paper or its Supplementary Information.

REFERENCES

Ajmal, M., Khan Rao, R. A. & Siddiqui, B. A. 1996 Studies on removal and recovery of Cr(VI) from electroplating wastes. *Water Research* **30** (6), 1478–1482. https://doi.org/10.1016/0043-1354(95)00301-0.

Al-Omair, M. A. & El-Sharkawy, E. A. 2007 Removal of heavy metals via adsorption on activated carbon synthesized from solid wastes. *Environmental Technology* **28** (4), 443–451. https://doi.org/10.1080/09593332808618808.

Al-Qodah, Z. & Shawabkah, R. 2009 Production and characterization of granular activated carbon from activated sludge. *Brazilian Journal of Chemical Engineering* **26**, 127–136. https://doi.org/10.1590/S0104-66322009000100012.

Alzaydien, A. S. 2009 Adsorption of methylene blue from aqueous solution onto a low-cost natural Jordanian Tripoli. *American Journal of Environmental Sciences* (5), 197–208. https://doi.org/10.3844/ajassp.2009.1047.1058.

Banerjee, S., Shraboni, M., Augustine, L., Joshi, S. R., Tamal, M. & Gopinath, H. 2016 Biosorptive uptake of Fe^{2+}, Cu^{2+} and As^{5+} by activated biochar derived from *Colocasia esculenta*: isotherm, kinetics, thermodynamics, and cost estimation. *Journal of Advanced Research* **7** (5), 597–610. https://doi.org/10.1016/j.jare.2016.06.002.

Bingxin, X., Jihong, Q., Wang, S., Xin, L., Hui, S. & Wenqing, C. 2020 Adsorption of phenol on commercial activated carbons: modelling and interpretation. *International Journal of Environmental Research and Public Health* **17** (3), 789–802. https://doi.org/10.3390/ijerph17030789.

Caetano, M., Valderrama, C., Farran, A. & Cortina, J. L. 2009 Phenol removal from aqueous solution by adsorption and ion exchange mechanisms onto polymeric resins. *Journal of Colloid and Interface Science* **338** (2), 402–409. https://doi.org/10.1016/j.jcis.2009.06.062.

Carvalho, M. F., Duque, A. F., Gonçalves, I. C. & Castro, P. M. L. 2007 Adsorption of fluorobenzene onto granular activated carbon: isotherm and bioavailability studies. *Bioresource Technology* (98), 3424–3430. https://doi.org/10.1016/j.biortech.2006.11.001.

Elboughdiri, N. 2018a Olive mill wastewater phenolic compounds adsorption onto active olive stones: equilibrium isotherms and kinetics study. *International Journal of Forensic Engineering* **4** (1), 31–46. https://doi.org/10.1504/IJFE.2018.094042.

Elboughdiri, N. 2018b Effect of time, solvent-solid ratio, ethanol concentration and temperature on extraction yield of phenolic compounds from olive leaves. *Engineering Technology & Applied Science Research* **8** (2), 2805–2808. https://doi.org/10.13140/RG.2.2.26002.81601.

Elboughdiri, N. 2020 The use of natural zeolite to remove heavy metals Cu (II), Pb (II) and Cd (II), from industrial wastewater. *Cogent Engineering* **7** (1782623), 1–13. https://doi.org/10.1080/23311916.2020.1782623.

ElHajam, M., Idrissi, N. K., Plavan, G. I., Abdel Halim, H., Mansour, L., Boufahja, F. & Zerouale, A. 2020 Pb^{2+} ions adsorption onto raw and chemically activated Dibetou sawdust: application of experimental designs. *Journal of King Saud University – Science* **32** (3), 2176–2189. https://doi.org/10.1016/j.jksus.2020.02.027.

Goel, J., Kadirvelu, K., Rajagopal, C. & Garg, V. K. 2005 Removal of lead (II) by adsorption using treated granular activated carbon: batch and column studies. *Journal of Hazardous Materials* **125** (1–3), 211–220. https://doi.org/10.1016/j.jhazmat.2005.05.032.

Iglesias-Carres, L., Mas-Capdevila, A., Bravo, F. I., Aragonès, G., Muguerza, B. & Arola-Arna, A. 2019 Optimization of a polyphenol extraction method for sweet orange pulp (*Citrus sinensis* L.) to identify phenolic compounds consumed from sweet oranges. *PLoS One* **19**, 1–17. https://doi.org/10.1371/journal.pone.0211267.

Indiamart. *Activated Carbon*. Available from: https://dir.indiamart.com/impcat/activated-carbon.html (accessed 19 December 2020).

Lima, I. M., McAloon, A. & Boateng, A. A. 2008 Activated carbon from broiler litter: process description and cost of production. *Biomass and Bioenergy* **32** (6), 568–572. https://doi.org/10.1016/j.biombioe.2007.11.008.

Liyana-Pathirana, C. & Shahidi, F. 2005 Optimization of extraction of phenolic compounds from wheat using response surface methodology. *Food Chemistry* **93**, 47–56. https://doi.org/10.1016/j.foodchem.2004.08.050.

Lütke, S. F., Igansi, A. V., Pegoraro, L., Dotto, G. L., Pinto, L. A. A. & Cadaval, T. R. S. 2019 Preparation of activated carbon from black wattle bark waste and its application for phenol adsorption. *Journal of Environmental Chemical Engineering* **7** (5), 103396. https://doi.org/10.1016/j.jece.2019.103396.

McGraw Hill. *Equipment Costs Plant Design and Economics for Chemical Engineers*. Available from: http://www.mhhe.com/engcs/chemical/peters/data/ (accessed 19 December 2020).

McKay, G. 1984 Adsorption of dyestuffs from aqueous solutions using the activated carbon adsorption model to determine breakthrough curves. *Chemical Engineering Journal and the Biochemical Engineering Journal* (28), 95–104. https://doi.org/10.1016/0300-9467(84)85020-0.

McMaster-CARR. *Choose a Category*. Available from: https://www.mcmaster.com/ (accessed 19 December 2020).

Mohanty, K., Das, D. & Biswas, M. N. 2005 Adsorption of phenol from aqueous solutions using activated carbons prepared from *Tectona grandis* sawdust by $ZnCl_2$ activation. *Chemical Engineering Journal* **115** (1–2), 121–131. https://doi.org/10.1016/j.cej.2005.09.016.

Mojoudi, N., Mirghaffari, N., Soleimani, M., Shariatmadari, H., Belver, C. & Bedia, J. 2019 Phenol adsorption on high microporous activated carbons prepared from oily sludge: equilibrium, kinetic and thermodynamic studies. *Scientific Report* **9**, 19352. https://doi.org/10.1038/s41598-019-55794-4.

Ng, C., Marshall, W. E., Rao, R. M., Bansode, R. R. & Losso, J. N. 2003 Activated carbon from pecan shell: process description and economic analysis. *Industrial Crops and Products* **17** (3), 209–217. https://doi.org/10.1016/S0926-6690(03)00002-5.

Ngah, W. W. S. & Hanafiah, M. A. K. M. 2008 Removal of heavy metal ions from wastewater by chemically modified plant wastes as adsorbents: a review. *Bioresource Technology* (99), 3935–3948. https://doi.org/10.1016/j.biortech.2007.06.011.

Omprakash, S., Dubasi, G. R., Nigus, G., Addis, E. & Firomsa, T. 2017 Sorption of phenol from synthetic aqueous solution by activated sawdust: optimizing parameters with response surface methodology. *Biochemistry and Biophysics Reports* **12**, 46–53. https://doi.org/10.1016/j.bbrep.2017.08.007.

Qiu, W. & Zheng, Y. 2007 Arsenate removal from water by an alumina-modified zeolite recovered from fly ash. *Journal of Hazardous Materials* (148), 721–726. https://doi.org/10.1016/j.jhazmat.2007.03.038.

RuiYan, W., Yong, W., XiaoYan, X., TuoPing, H., JianFeng, G. & FuQiang, A. 2019 Selective adsorption and removal ability of pine needle-based activated carbon towards Al(III) from La(III). *Journal of Dispersion Science and Technology* **40** (2), 186–191. https://doi.org/10.1080/01932691.2018.1464933.

Solgi, M., Tahereh, N., Shahyar, A. & Bahram, N. 2017 Synthesis and characterization of novel activated carbon from Medlar seed for chromium removal: experimental analysis and modeling with artificial neural network and support vector regression. *Resource-Efficient Technologies* **3** (3), 236–248. https://doi.org/10.1016/j.reffit.2017.08.003.

Srivastava, V. C., Swamy, M. M., Mall, I. D., Prasad, B. & Mishra, I. M. 2006 Adsorptive removal of phenol by bagasse fly ash and activated carbon: equilibrium, kinetics and thermodynamics. *Colloids and Surfaces A: Physicochemical and Engineering Aspects* **272** (1–2), 89–104. https://doi.org/10.1016/j.colsurfa.2005.07.016.

Sumon, M. R., Cheong, S. Y., Shammya, A., Nikdalila, R., Muhammad, S., Bakar, A., Rahman Saidur, R., Taweekun, J. & Azad, A. 2020 Preparation of activated carbon from biomass and its' applications in water and gas purification, a review. *Arab Journal of Basic and Applied Sciences* **27** (1), 208–238. https://doi.org/10.1080/25765299.2020.1766799.

Sun, Q. & Yang, L. 2003 The adsorption of basic dyes from aqueous solution on modified peat-resin particle. *Water Research* **37** (7), 1535–1544. https://doi.org/10.1016/S0043-1354(02)00520-1.

Witek-Krowiak, A. 2013 Application of beech sawdust for removal of heavy metals from water: biosorption and desorption studies. *European Journal Wood Production* **71**, 227–236. https://doi.org/10.1007/s00107-013-0673-8.

Wiwid, P. P., Azlan, K., Siti, N. M., Che, F. I., Azmi, M., Norhayati, H. & Illyas, M. I. 2014 Biosorption of Cu(II), Pb(II) and Zn(II) ions from aqueous solutions using selected waste materials: adsorption and characterization studies. *Journal of Encapsulation and Adsorption Sciences* **4** (1), 25–35. https://doi.org/10.4236/jeas.2014.41004.

Woo-seok, S. 2017 Adsorption characteristics of phenol and heavy metals on biochar from Hizikia fusiformis. *Environmental Earth Sciences* **76** (782), 200–215. https://doi.org/10.1007/s12665-017-7125-4.

First received 21 November 2020; accepted in revised form 22 December 2020. Available online 8 March 2021